RESEARCH ARTICLE

CHEMISTRY & BIODIVERSITY

A Drug Repurposing Approach to Identify Therapeutics by Screening Pathogen Box Exploiting SARS-CoV-2 Main Protease

Rashmi Tyagi,[a] Anubrat Paul,[a] V. Samuel Raj,[a] Krishna Kumar Ojha,[b] Sunil Kumar,*[c]
Aditya K Panda,[d] Anurag Chaurasia,[e] and Manoj Kumar Yadav*[a, f]

[a] Center for Drug Design Discovery and Development (C4D), SRM University, Delhi-NCR
Sonepat – 131 029, Haryana, India
[b] Department of Bioinformatics, Central University of South Bihar, Gaya-824 236, Bihar, India
[c] ICAR-Indian Agriculture Statistical Research Institute, New Delhi, India 110012, e-mail: skybiotech@gmail.com
[d] Department of Biosciences and Bioinformatics, Khallikote University, Berhampur 761008, Odisha, India
[e] ICAR-Indian Institute of Vegetable Research, Varanasi 221305, UP, India
[f] Department of Biomedical Engineering, SRM University, Delhi-NCR, Rajiv Gandhi Education City, Sonepat
131 029, Haryana, India, e-mail: manojiids@gmail.com

Coronavirus disease-19 (COVID-19) is caused by severe acute respiratory syndrome coronavirus -2 (SARS-CoV-2) and is responsible for a higher degree of morbidity and mortality worldwide. There is a smaller number of approved therapeutics available to target the SARS-CoV-2 virus, and the virus is evolving at a fast pace. So, there is a continuous need for new therapeutics to combat COVID-19. The main protease (M^{pro}) enzyme of SARS-CoV-2 is essential for replication and transcription of the viral genome, thus could be a potent target for the treatment of COVID-19. In the present study, we performed an *in-silico* screening analysis of 400 diverse bioactive inhibitors with proven antibacterial and antiviral properties against M^{pro} drug target. Ten compounds showed a higher binding affinity for M^{pro} than the reference compound (N3), with desired physicochemical properties. Furthermore, in-depth docking and superimposition revealed that three compounds (MMV1782211, MMV1782220, and MMV1578574) are actively interacting with the catalytic domain of M^{pro}. In addition, the molecular dynamics simulation study showed a solid and stable interaction of MMV178221-M^{pro} complex compared to the other two molecules (MMV1782220, and MMV1578574). In line with this observation, MM/PBSA free energy calculation also demonstrated the highest binding free energy of -115.8 kJ/mol for MMV178221-M^{pro} compound. In conclusion, the present *in silico* analysis revealed MMV1782211 as a possible and potent molecule to target the M^{pro} and must be explored *in vitro* and *in vivo* to combat the COVID-19.

Keywords: COVID-19, virtual screening, molecular docking, ADMET, molecular dynamics simulations.

1. Introduction

The first incidence of severe acute respiratory syndrome coronavirus-2 (SARS-CoV-2) was reported in December 2019 in the Wuhan City of Hubei Province, China,[1–3] and later on, it spreads worldwide. The World Health Organization (WHO) on March 11, 2020, has announced the new coronavirus (COVID-19) outbreak a worldwide pandemic.[4] SARS-CoV-2 is a positive-sense single-stranded RNA virus of 26–32 kilobases and possesses 14 open reading frames (ORFs) encoding 27 proteins of variable length. The

one-third portion of the genome produces an array of structural proteins, namely surface glycoprotein (S), a small envelope protein (E), matrix protein (M), and nucleocapsid protein (N); and accessory proteins (3a, 3b, 6, 7a, 7b, 8, 9b, 9c and 10). The spike surface glycoprotein is responsible for the binding of the virus to the host cell. The spike protein interacts with the angiotensin-converting enzyme 2 (ACE2) of the host and is responsible for viral entry inside the cell. Apart from that, the virus produces an array of non-structural proteins that are directly related to the survival and pathogenicity of SARS-CoV-2. The ongoing research is

utilizing these structural and non-structural proteins for developing effective therapeutics. An array of computational studies has been conducted to examine the inhibitory potential of polyphenols viz. curcumin as antivirals.[5,6] The studies shows that curcumin play a role in hindering the formation of S Protein-ACE2 complexes.[7] Another compound, 8-Hydroxydihydro-sanguinarine shows a promising result as an anti-COVID-19 compound as it distorts the α-helix in the secondary structure RBD site of S protein, and interferes in the coupling of S protein and ACE2 receptors.[8]

Protease enzyme is also an integral part of non-structural proteins essential for viral replication by mediating the maturation of viral replicase complex.[9] The two proteases, namely papain-like protease (PL^{pro}) and main protease (M^{pro}) co-translationally cleave the two polypeptides (pp1a, and pp1b) into mature non-structural proteins.[10,11] The release of functional polypeptides from the polyproteins involves extensive proteolytic processing, which is mainly accomplished by SARS-CoV-2 M^{pro}. SARS-CoV-2 M^{pro} processes and digest the polyprotein at 11 conserved sites, starting with the autolytic cleavage of this enzyme itself from pp1a and pp1ab.[12,13] Evolutionary study based on SARS-CoV-2 M^{pro} enzyme reveals their conservation across the entire coronaviridae subfamily. The M^{pro} plays a crucial role in the viral life cycle by controlling the viral replication and transcription[10] and thus could be an attractive target for designing therapeutics.

Drug repurposing is an exciting approach to design and check the efficacy of inhibitors against previously unknown targets. The inhibition potentials of chloroquine, hydroxychloroquine drug compounds have not been reported to target COVID-19 protease *in vitro*.[14] In the present study, we have applied an integrated approach to identify the key amino acid residues present at the active site of M^{pro}. In the next step, a library of compounds with known antibacterial and antiviral properties from the pandemic box were screened to test their efficacy as a potent inhibitor against SARS-CoV-2 M^{pro}.

2. Methodology

2.1. Protein Structure Retrieval

The three-dimensional crystal structure of the main protease (M^{pro}) of SARS-CoV-2 complexed with N3 (PDB ID: 6LU7) is determined using X-ray diffraction technique.[10] The 3D structure is of 2.16 Å resolution

and downloaded from protein data bank.[15] The other two M^{pro} structures: complexed with N1 (PDB ID: 1WOF) and alpha ketoamide (PDB ID: 6YNQ) ligands are having resolution of 2.00 Å and 1.80 Å, respectively.[16,17] Both the structures are predicted using X-ray diffraction techniques. The ligand-receptor complexes were preprocessed to make them suitable for study. The preprocessing steps include the removal of solvent molecules and accessory ligands. Later on, different structural features of the M^{pro} receptor, including their superimposition and the involvement of amino acids in defining the active site, were studied using Chimera, an open-source visualization software.[18]

2.2. Active Site Prediction

The SARS-CoV-2 M^{pro} protein interacts with various small molecules at its active site and performs biological functions. Identification of the main binding site is a crucial step in computer-aided drug design. The possible binding pockets were detected using the Computed Atlas of Surface Topography of proteins (CASTp) server,[19,20] which can locate, delineate, and measure a given protein's geometric and topological properties structure.

2.3. Ligand Preparation

The pathogen box, available at Medicines for Malaria Venture (MMV), collects over 400 diverse drug compounds against different pathogens (https://www.mmv.org/mmv-open/archived-projects/pathogen-box). These compounds consist of 201 antibacterial, 153 antivirals, and 46 antifungals with a diverse mechanism of action.[21] The compounds have not been tested against any target of COVID-19. The 3D structure of MMV's Pathogen Box compounds was constructed taking ACD/ChemSketch public domain software (http://www.acdlabs.com/ resources/ freeware/ chemsketch/) in MOL file. Compounds were edited and optimized using the Avogadro tool.[22] Open Babel, a chemical toolbox, was employed to convert ligand 3D structures in suitable file formats required for screening.[23]

2.4. Virtual Screening and ADMET Evaluation

Screening is a crucial step in computer-aided drug design to identify hit compounds based on shape, size, and ligand-receptor interaction. It records the activity of compounds at the active site of the

receptor. We have used PyRx virtual screening tool to screen library compounds. PyRx is open-source screening software to screen libraries of compounds {Dallakyan, 2015 #54} (Dallakyan and Olson 2015).

The molecular properties and drug-likeness score of MMV compounds were investigated using Molsoft (http://molsoft.com/mprop/P) to evaluate their pharmacological and biological properties. Lipinski's rule of five (Ro5) consists of HBA/ HBD value up to 10 and 5, respectively; MW less than 500, LogP value less than 5, and total BBB and drug-likeness score.[24]

2.5. Molecular Interaction

Docking experiments involve different steps of ligand preparation, receptor preparation, grid box creation, and docking. AutoDock Vina software was used for simulation purposes.[25] The ligand preparation step involves the generation of ligand conformers, charges, and identification of a number of rotatable bonds. M^{pro} receptor protein (PDB ID: 6LU7) is downloaded from RCSB PDB repository.[26] The ligand N3 was removed from the downloaded 3D structure using Chimera software.[18] Water molecules and heteroatoms were removed from the receptor molecule using ADT.[27] A Grid box is prepared around the receptor with dimensions $70 \times 80 \times 70$ XYZ points using a grid spacing of 1 Å, and the grid center is situated at XYZ coordinates -27.211, 11.241, and 58.511, respectively. The molecular docking is performed using default settings were applied with GA run to 300. The best-docked conformations were further selected for studying their dynamics at the nanoscale.

2.6. Molecular Dynamics Simulation Set Up

The procured hit compounds were subjected to molecular dynamics (MD) simulation experiments to study their interaction dynamics taking compound N3 as a control. The receptor protease (PDB ID:6LU7) was processed with Chimera software, and their topologies were generated employing GROMOS53a6 force field[28] implemented in Groningen Machine for Chemical Simulations (GROMACS 5.4.1) software.[29] Ligands topologies were generated utilizing the PRODRG server.[30] The M^{pro} protein is surrounded by a Dodecahedron box that was created using the edit conf module and with a 10 Å distance from the edges. A simple point charge water model (SPC216) is used to study their dynamics, and later on the system is neutralized by adding the counterions. The energy minimization step includes the steepest descent algorithm at 10,000 steps with an upper force limit lower than 1000 kJ/mol to stabilize the system. Later on, the system is equilibrated using number of particles, volume and temperature (NVT), and number of particles, pressure and temperature (NPT) at 100 ps at 300 k and 100 ps at a pressure of 1 bar maintained by Parrinello-Rahman barostat, constraining the protein backbone.[31] Linear Constraint Solver for Molecular Simulations (LINCS)[32] algorithm was used to restrain heavy atom bonds and their respective hydrogen atoms. Particle Mesh Ewald (PME) was utilized to compute the long rage electrostatic interaction taking a cut-off distance of 12 Å for Coulombic and van der Waals interactions.[33] MD simulations were performed up to 50 ns, storing the coordinate data for every 2 fs. We evaluated the simulation outputs by using XMGRACE[34] and Chimera software.[18]

3. Results and Discussion

SARS-CoV-2 infections develop several clinical complications such as pneumonia, acute kidney injury, heart problems, organ failure, blood clots, and secondary bacterial and viral infections.[35] Because of its dissimilarity to its host, M^{pro} of SARS-CoV-2 is an appealing therapeutic target, and it also plays a critical function in the processing of polyproteins translated from viral RNA. The present study identified and characterized the most potent inhibitors available in the Pathogen Box as a possible therapeutic target against the main protease using drug repurposing dimensions.
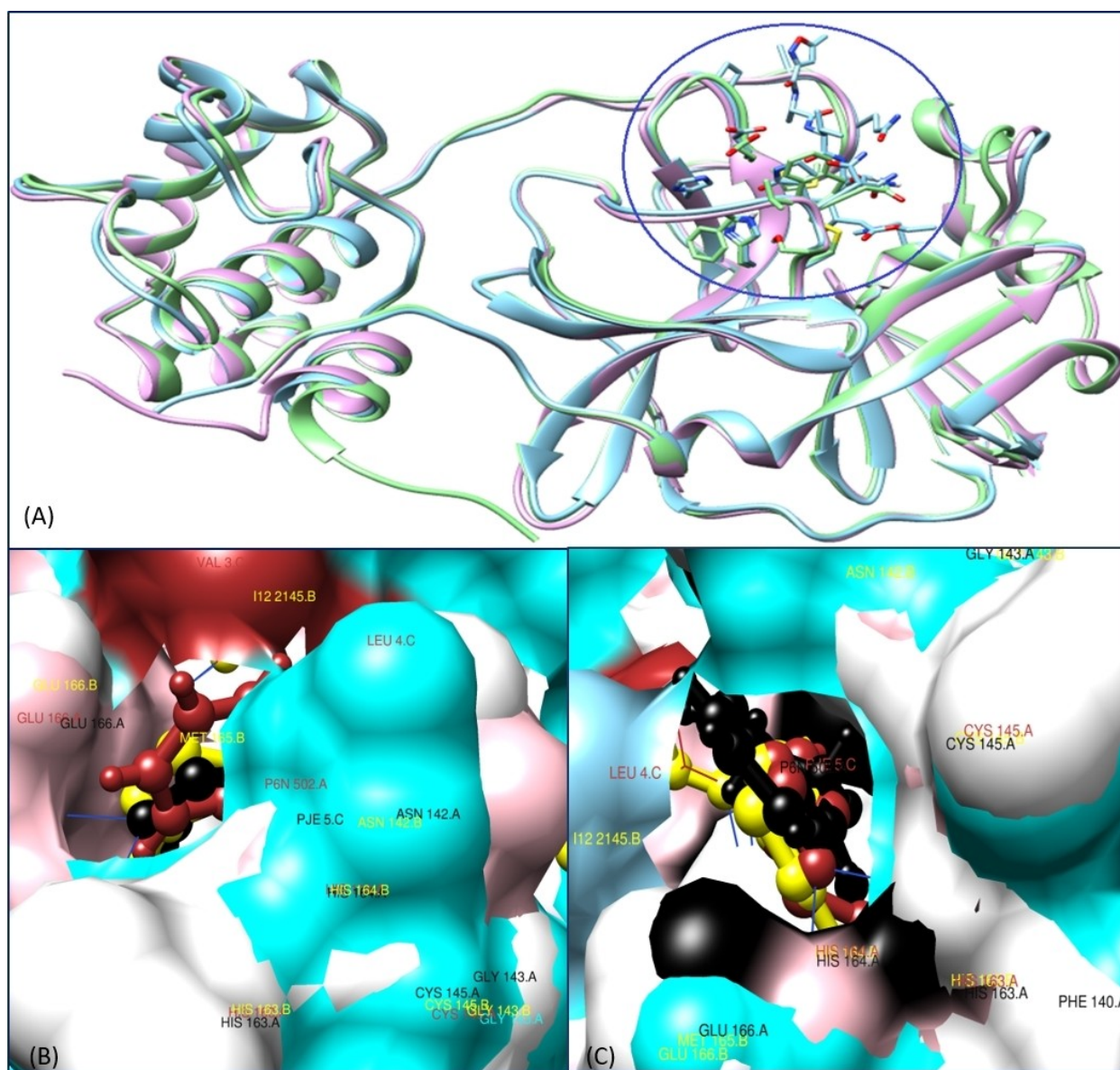
3.1. Structural Analysis of M^{pro} Drug Target

M^{pro} plays a major role in the replication and transcription of the virus inside human cells.[10] SARS-CoV-2 M^{pro} protein consists of 306 amino acids and shows 96 percent identity with the M^{pro} of SARS-CoV virus of the same lineage. The availability of the three-dimensional structure of M^{pro} provides an opportunity to look inside the structure for its activity and also pave a way to identify potential drug candidates that can able to disrupt its activity. The 3D structure of M^{pro} co-crystallized with Michael acceptor inhibitor, N3 is taken from Protein Data Bank (PDB ID: 6LU7).[10] The structural analysis and visualization show that it exists in a dimer form where each monomer is a protomer and is composed of three domains: domain I (8-101 amino acid residues), domain II (102-184), and domain III (201-303). Domain I and II show antiparallel β-barrel structure, and domain III constitutes a globular

structure with antiparallel arranged five α-helices. A long loop region usually comprises 15 amino acid residues that connect domain II to domain III.

The other two available 3D structures of M^pro protein (PDB ID-1WOF and 6YNQ) complexed with N1 and α-ketoamide inhibitors are taken from the protein database.[16,17] We did a structural analysis of available three 3D structures along with their respective ligands using Chimera software. An overlay of the structures of SARS-CoV-2 M^pro-N3 and M^pro-α-ketoamide and

SARS-CoV-1 M^pro-N1 show that all the three inhibitors occupy the same binding site of M^pro with nearly similar binding modes as evident from *Figure 1*. The structural superimposition result clearly shows a high degree of similarity between SARS-CoV-2 M^pro-N3 complex (PDB ID-6LU7) and SARS-CoV-2 M^pro with α-ketoamide inhibitor in terms of their root mean square deviation of 0.406 Å compared to main protease co-crystallized with N1 inhibitors (RMSD:0.671). However, the surface loops and α-helices of domain III are


Figure 1. Structural Analysis of SARS-CoV-2 M^pro complexed with inhibitors. (A) Superposition of crystal structures of M^pro shown in ribbon form 6LU7 (Pink), 1WOF (Blue), 6YNQ (Lime green) co-crystallized with their respective ligands, N3, N1, and alpha ketoamide inhibitor in stick forms with atom level color, (B) and (C) Surface view of M^pro active sites where the active site of 6LU7 (cyan), 1WOF (white) and 6YNQ (pink) along with their ligands: N3 (red), N1 (yellow) and alpha ketoamide (black). Chimera software is used for visualizations.

showing large variations while the substrate-binding pockets located in a cleft between domains I and II are perfectly superimposed and show the highest level of conservations among the three M^pro structures. It is also evident that N3, N1, and α-ketoamide inhibitors are present in a similar binding mode at the conserved binding pockets. This will pose more confidence that disrupting the M^pro active site by drug repurposed inhibitors may disrupt its normal course of action and results in decreased SARS-CoV-2 activity.

3.2. Exploring the Potential Binding Site of M^pro Receptor

We performed a ligand-independent binding site search for M^pro protein using the CASTp server to bring more robustness in confirming the main binding site before the screening. The output result showed a total of 38 binding pockets and other sub-pockets. The ligand, in general, interacts with the binding pocket having the largest cavity. The solvent-accessible surface area is 224 $Å^2$, with a volume of 180 $Å^3$ for the largest binding pocket (*Figure 2*). The amino acid residues namely THR24, THR25, THR26, LEU27, HIS41, THR45, SER46, MET49, PHE140, LEU141, ASN142, GLY143, SER144, CYS145, HIS163, MET165, GLU166, HIS172 of chain A; and VAL3, LEU4 of chain C are mainly involved in constituting main binding pocket of COVID-19 M^pro receptor. The presence of conserved residues, HIS41 and CYS145, at the catalytic dyad at
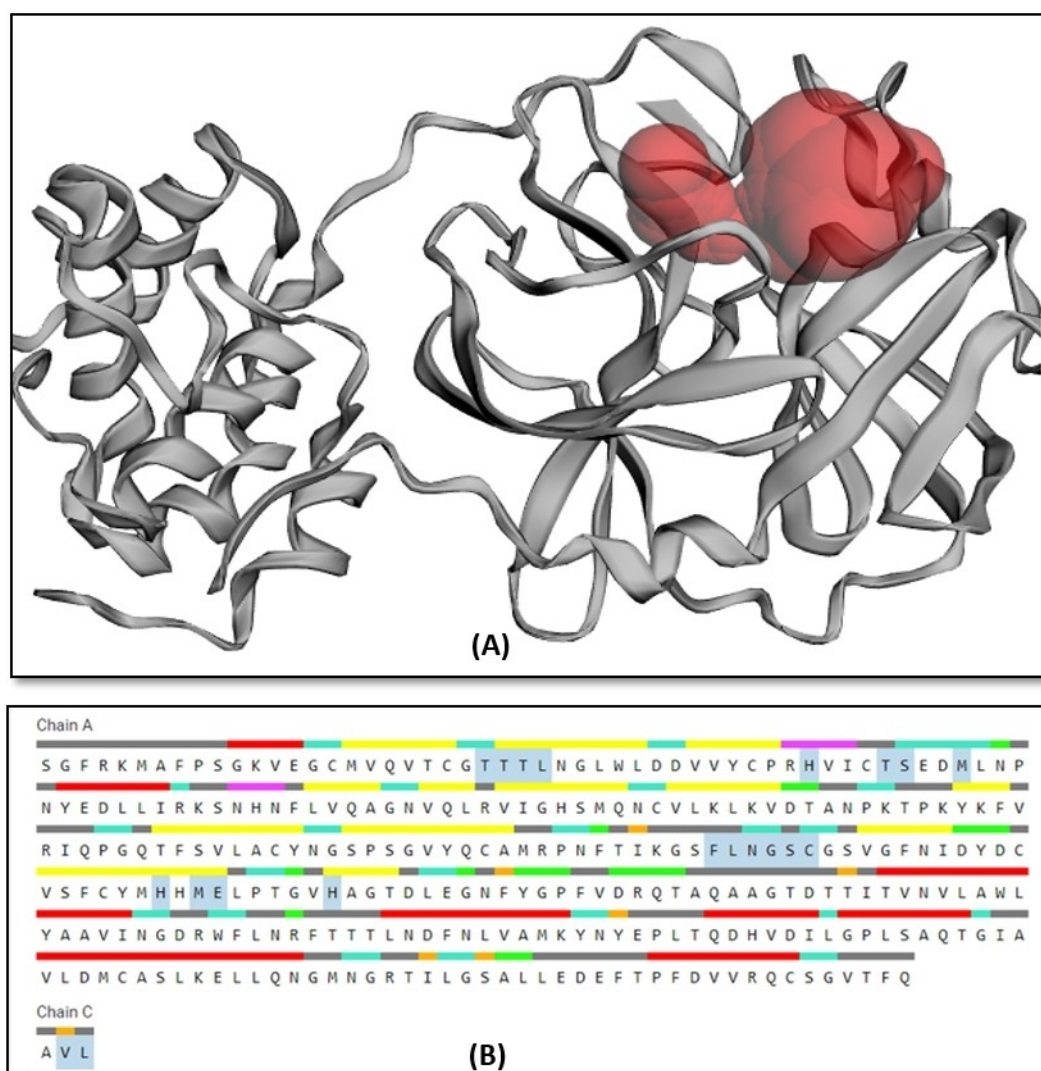
Figure 2. Binding site prediction using the CASTp server (A) Active site pocket of M^pro shown in red spheres on residues (B) secondary structure elements is visible in different colors. Amino acid residues present at the largest binding pocket are highlighted in cyan color.

the substrate-binding site of M^{pro} validates our hypothesis of active site prediction.

3.3. Virtual Screening of Compounds in Pathogen Box

Screening is a computational technique that can identify bioactive hit candidates from a collection of small compound libraries. PyRx is used to identify potential compounds against M^{pro} enzyme of SARS-CoV-2. We have selected 400 diverse bioactive inhibitors, that were previously useful for targeting other diseases, from the Pathogen Box available at Medicines for Malaria Venture for screening against the target enzyme. Jin et al. reported that a small molecule N3 forms a stable complex with M^{pro} protein.[10] So, we have included the N3 inhibitor as a control to screen 400 diverse compounds to validate our screening parameters. The presence of N3 inhibitor in the screening result successfully cross validates our hypothesis. Twelve compounds did not show any binding, and the remaining compounds bind at the main cavity with differential binding energies of −4.2 to −9.0 kcal/mol. We have used the binding energy of our control (−6.0 kcal/mol) as a cut-off criterion to filter our screening compounds (*Table 1*). Total ten compounds having higher binding affinity to our control are taken further for in-depth study.

3.4. Study of Physicochemical Properties of Screened Compounds

The interaction of a compound with its physical environment determines its physicochemical properties responsible for the biological activity of compounds. The drug-likeness score is calculated by considering partition coefficient (log P), molecular weight, number of hydrogen donors, number of hydrogen acceptors, and number of violations to Lipinski's rule (*Table 1*). The calculated molecular weight, hydrogen bond acceptors, hydrogen bond donors of obtained compounds are 422 to 957, 2 to 7, and 1 to 3, respectively. The molecular polar surface area is directly related to the passive transport of drugs through membranes, and their values lie within the range of 26.92–160.96 Å^2. The contribution of each functional group & structural arrangement helps to determine the lipophilic character and is positively associated with the permeability and bioavailability of drugs. The log P values of drugs lie between −0.58 and 6.11. The structural and molecular properties of a particular compound are similar to the known drugs or not, is determined by the Drug-likeness score,

which lies in the range of −0.41 to 2.68. The screened drugs are likely to be orally active as they agree with Lipinski's rules with fewer violations and the drug-likeness score. These compounds classify the basic drug criterion and are used in the next step of the drug design process.
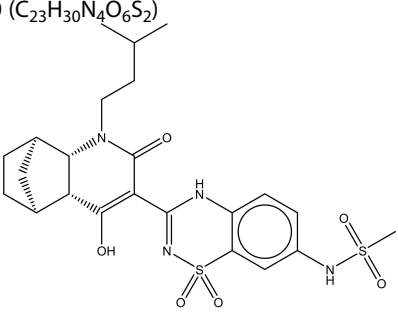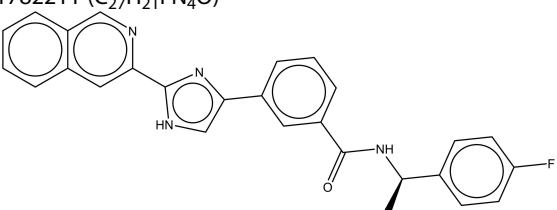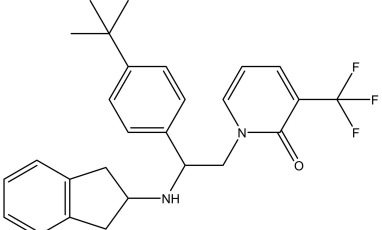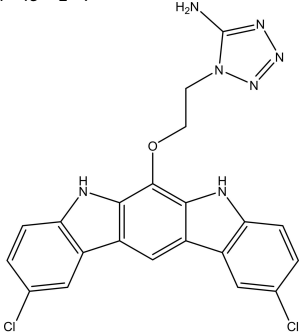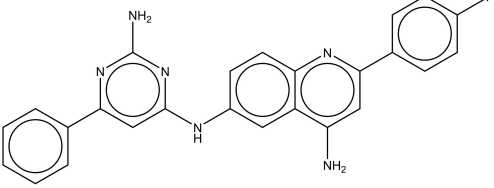
3.5. Interaction of Screened Drugs with M^{pro} Receptor

The selected ten hits from the screening experiments are further scrutinized using docking studies with stringent parameters. AutoDock Vina software was used for docking selected compounds against the M^{pro} protein. We want to check all the possibilities whether the ligand conformers bind to the primary binding site or additional binding site, that's why we have set up a molecular grid covering the whole receptor. The docking result showed a more or less similar trend in binding energy compared to PyRx screening tool (*Table 2*). The docking studies using Vina software shed more light on binding poses and interactions of ligands at the active site of M^{pro} receptor in terms of hydrogen bonding and other non-bonded interactions.
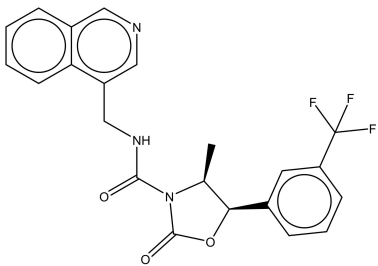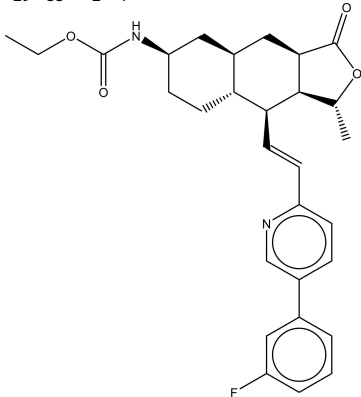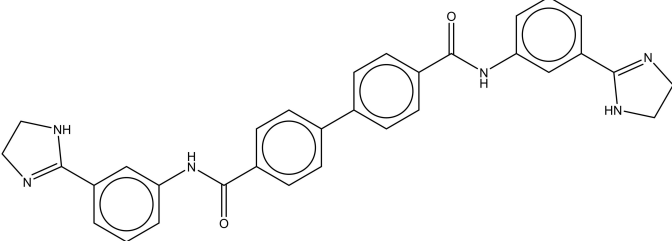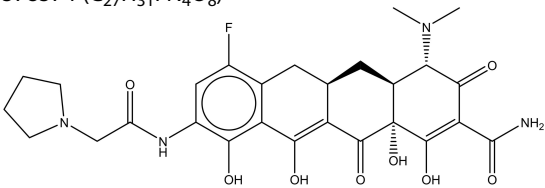
MMV1782220 ligand docked at the main binding site of M^{pro} receptor of SARS-CoV-2 with the binding energy of −8.2 kcal/mol. The amino acid residues involved in the hydrophobic interactions are HIS41, THR24, THR25, THR45, GLY143, LEU141, ASN142, GLU166, HIS163, MET165, where THR45 and GLY143 amino acids of receptor show hydrogen bonding with inhibitors. The compound MMV1782211 interacted with residues THR25, THR26, MET49, ARG188, GLN189, MET165, PRO168 of the receptor with docking affinity −8.9 kcal/mol. Similarly, MMV1634393 (−8.7 kcal/mol) and MMV1633966 (−8.8 kcal/mol) interact with GLN110, VAL202, THR292, PRO293, PHE294, ILE249; and ARG131, LYS137, ASP197, THR198, THR199, ASN238, LEU286, LEU287, residues, respectively, one hydrogen bond generated by MMV1633966 with residue THR199. Another compound, MMV1593541 showed interactions with residues, namely GLU14, GLN19, GLY70, GLY71, VAL73, GLY120, SER121, with a binding affinity of −8.7 kcal/mol.

The amino acid residues, namely LYS137, THR199, TYR237, TYR239 and GLU290 are involved in holding MMV1593533 ligand at the binding cavity of M^{pro} receptor with a binding energy of −8.3 kcal/mol and with one hydrogen bond made by THR199. The interaction of M^{pro} receptor and MMV1593515 involves TYR237, LYS137, TYR239, ASP289, MET276 with an

Table 1. Calculation of ADMET properties of screened compounds.
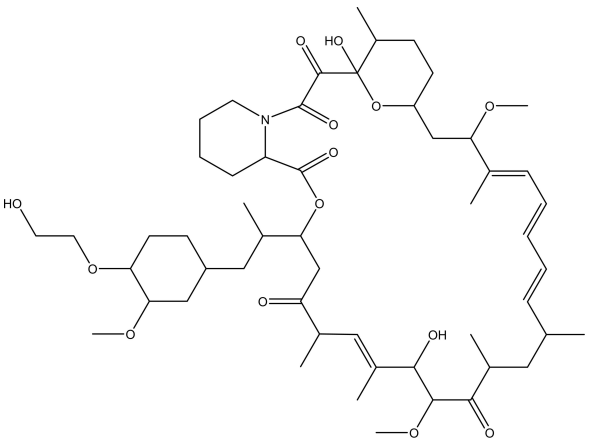
Compounds	Molecular Properties and Drug-likeness Properties	Value
MMV1782220 ($C_{23}H_{30}N_4O_6S_2$)	Molecular weight	522.16
	Number of HBA	7
	Number of HBD	3
	MolLogP	2.50
	MolPSA	126.41
	Drug-likeness model score	0.75
MMV1782211 ($C_{27}H_{21}FN_4O$)	Molecular weight	436.17
	Number of HBA	3
	Number of HBD	2
	MolLogP	5.55
	MolPSA	52.25
	Drug-likeness model score	0.43
MMV1634393 ($C_{27}H_{29}F_3N_2O$)	Molecular weight	454.22
	Number of HBA	2
	Number of HBD	1
	MolLogP	6.60
	MolPSA	26.96
	Drug-likeness model score	1.26
MMV1633966 ($C_{21}H_{15}Cl_2N_7O$)	Molecular weight	451.07
	Number of HBA	4
	Number of HBD	4
	MolLogP	4.51
	MolPSA	87.44
	Drug-likeness model score	−0.41
MMV1593541 ($C_{25}H_{19}FN_6$)	Molecular weight	422.17
	Number of HBA	3
	Number of HBD	5
	MolLogP	6.11
	MolPSA	76.64
	Drug-likeness model score	0.14
MMV1593533 ($C_{22}H_{18}F_3N_3O_3$)	Molecular weight	429.13

Table 1. (cont.)

Compounds	Molecular Properties and Drug-likeness Properties	Value
	Number of HBA	4
	Number of HBD	1
	MolLogP	4.68
	MolPSA	55.82
	Drug-likeness model score	0.36
MMV1593515 ($C_{29}H_{33}FN_2O_4$)	Molecular weight	492.24
	Number of HBA	5
	Number of HBD	1
	MolLogP	5.85
	MolPSA	63.59
	Drug-likeness model score	0.65
MMV1580853 ($C_{32}H_{28}N_6O_2$)	Molecular weight	528.23
	Number of HBA	4
	Number of HBD	4
	MolLogP	6.12
	MolPSA	90.38
	Drug-likeness model score	0.46
MMV1578574 ($C_{27}H_{31}FN_4O_8$)	Molecular weight	558.21
	Number of HBA	10
	Number of HBD	7
	MolLogP	−0.58
	MolPSA	148.71
	Drug-likeness model score	2.68
MMV639951 ($C_{53}H_{83}NO_{14}$)	Molecular weight	957.58

Table 1. (cont.)

Compounds	Molecular Properties and Drug-likeness	
	Properties	Value
	Number of HBA	14
	Number of HBD	3
	MolLogP	5.26
	MolPSA	160.96
	Drug-likeness model score	0.65

Table 2. Interaction of selected drug compounds at the active site of Mpro receptor of SARS-CoV-2.

S. No.	MMV ID	Binding Affinity (kcal/mol)	pIC_{50} (µM)	Interacting Residues	Hydrogen Bonds
1	MMV1782220	−8.2	0.97	THR45, HIS41, THR25, THR24, GLY143, LEU141, ASN142, GLU166, HIS163, MET165	THR45, GLY143
2	MMV1782211	−8.9	0.30	THR25, THR26, MET49, ARG188, GLN189, MET165, PRO168,	0
3	MMV1634393	−8.7	0.42	VAL202, GLN110, THR292, PRO293, PHE294, ILE249,	0
4	MMV1633966	−8.8	0.35	LEU286, LEU287, THR199, THR198, ASN238, ARG131, ASP197, LYS137	THR199
5	MMV1593541	−8.7	0.42	GLU14, SER121, GLY70, GLY71, GLY120, VAL73, GLN19	0
6	MMV1593533	−8.3	0.81	TYR237, THR199, TYR239, LYS137, GLU290	THR199
7	MMV1593515	−8.2	0.97	TYR237, LYS137, TYR239, ASP289, MET276	MET276
8	MMV1580853	−8.3	0.81	TYR239, LYS137, LEU287, LEU286, LYS5	LEU287
9	MMV1578574	−8.4	0.69	HIS41, MET49, MET165, HIS164, GLU166, GLY143,	HIS164
10	MMV639951	−7.9	1.60	ARG188, ASN153, TYR54, ARG40, GLU55, ASN180, ASN84, ARG105, GLU178	ARG40, TYR54, ARG188
11	N3 compound (control)	−6.0	39.72	PHE294, ASN151, SER158, VAL104, GLN110	0

affinity of −8.2 kcal/mol. MET276 shows hydrogen bonding with MMV1593515.

TYR239, LYS137, LEU287, LEU286, LYS5 interacts with MMV1580853 ligand at the main active site with binding affinity −8.3 kcal/mol. The ligand showed a hydrogen bonding interaction with LEU287.

The docking energy of MMV1578574 with the receptor is −8.4 kcal/mol, and the interacted residues are HIS41, MET49, MET165, HIS164, GLU166, GLY143, along with one hydrogen bond involving residue HIS164. The close contact amino acid residues, namely ARG40, TYR54, GLU55, ASN84, ARG105, ASN153, GLU178, ASN180 and ARG188 are showing interactions

with MMV639951 compound with −7.9 kcal/mol, and it also forms a strong hydrogen bond network with ARG40, TYR54, ARG188. Later on, we obtained the corresponding IC_{50} (µM) values using the compound's binding affinity X (kcal/mol):

$$IC_{50} = 10^{X/1.3633} \times 10^{-6}$$

A complete list of the predicted values selected compounds is given in the *Table 2*.

### 3.6 In-Depth Binding Analysis of Docked Compounds at the Main Active Site of M^{pro} Receptor Protein

The superimposition of all the docked compounds obtained from the docking experiment showed that their minimum energy conformers bind at the main active site and additional binding sites with a differential binding affinity. The in-depth analysis revealed that only three compounds, MMV1782220, MMV1782211, and MMV1578574, were found at the main active site cavity beside the N3 compound, as visible from *Figure 3*. Apart from that, other ligands are binding to some other binding cavities, suggesting the presence of additional cavities in the receptor.

The compounds found to be present at the main cavity are further selected for in-depth interaction study. The selected three compounds show a signifi-cant binding affinity at the M^{pro} active site. The network of hydrogen bonding patterns is present between ligands and receptors. The presence of an array of hydrophobic interactions is also responsible for holding these ligands at the main binding pocket of M^{pro} receptor (*Figure 4*). Hence it is clear from the docking study that three compounds (MMV1782211, MMV1782220, and MMV1578574) are showing satisfactory interactions at the main active site of M^{pro} drug target. This experiment needs some additional validation in terms of pose stability and interaction stability. The stability and reliability of complexes were further checked by conducting molecular dynamics simulations.
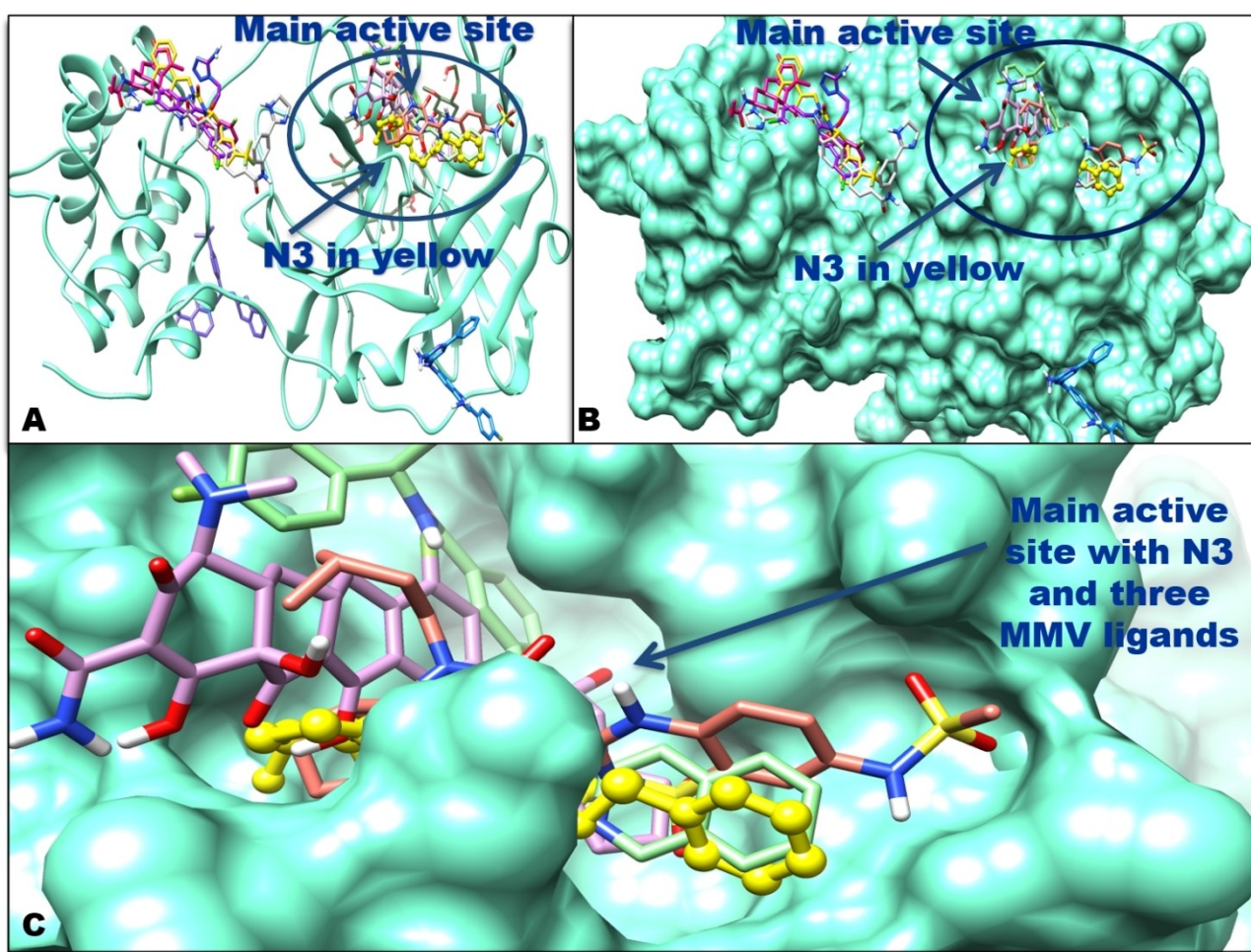
Figure 3. Binding of ligands at the M^{pro} receptor protein. (A) Secondary structure representation B) Surface view; Only three ligands (MMV1782220 MMV1782211 and MMV1578574) out of 10 binds at the main active site of the receptor (C) enlarged surface view of the main active site showing three ligands at main active site pocket along with N3 (yellow color). Chimera software is used for visualization of complexes.
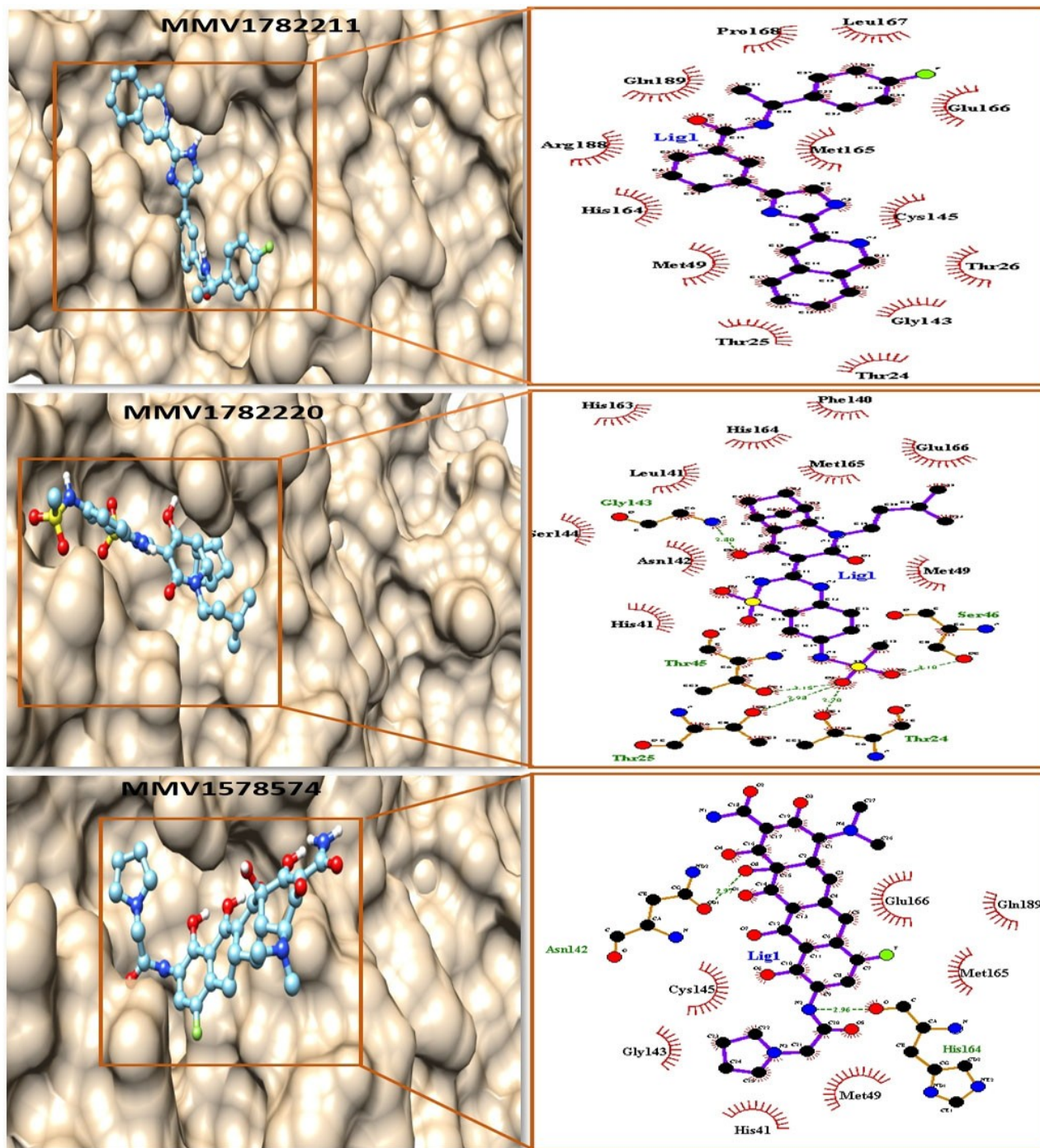
Figure 4. Binding modes of minimum energy conformers after docking experiments of MMV compounds: 3D structure of M^{pro} protein is shown as molecular surface models in Tan color and ligands are represented as ball and stick models on the left-hand side using Chimera software while ligand-receptor interactions and their close contact residues are visible on the right-hand side pane using LigPlot program where hydrogen bonds are labeled in green color.

3.7. Molecular Dynamics Simulation Analysis of Selected Complexes

The primary objective of performing the MD simulation experiments is to assess the binding stability and dynamics of selected three compounds at the binding pocket of M^{pro} receptor. The four complexes (M^{pro}–N3, M^{pro}-MMV1782220, M^{pro}-MMV1782211, and M^{pro}-MMV1578574) were undergone simulation experiments individually up to the duration of 50 ns to check their stability. The output results of MD simulation experiments were examined in terms of their RMSD values, RMSF, hydrogen bond, solvent-accessible area, and radius of gyration to assess their individual and complex stability. Average RMSD analysis indicate that the M^{pro} structure is more stabilized upon binding with selected ligands, and their average RMSD varies from 2.2 to 3.7 Å, as shown in *Figure 5(A)*. Our

comparative analysis showed that the average RMSD fluctuations of MMV1782211 complex were the lowest and showed comparable synchrony with the reference M^{pro}-N3 complex. The average RMSD fluctuations of this complex are found to be even more stable than the reference one.

The RMSF analysis provides more detailed information about amino acid motions in M^{pro} receptor upon binding of selected compounds. RMSF fluctuations concerning amino acid residue numbers were plotted from the 50 ns trajectories (*Figure 5(B)*). The convergence of the simulation towards equilibrium can also be inferred from the relaxation of the structure. The RMSF are captured about each atom about its average positions. The result shows insight into the flexible regions of the protein, and corresponds to the crystallographic b-factors (temperature factors). The RMSF profile shows that the residues: LEU30, CYS38,
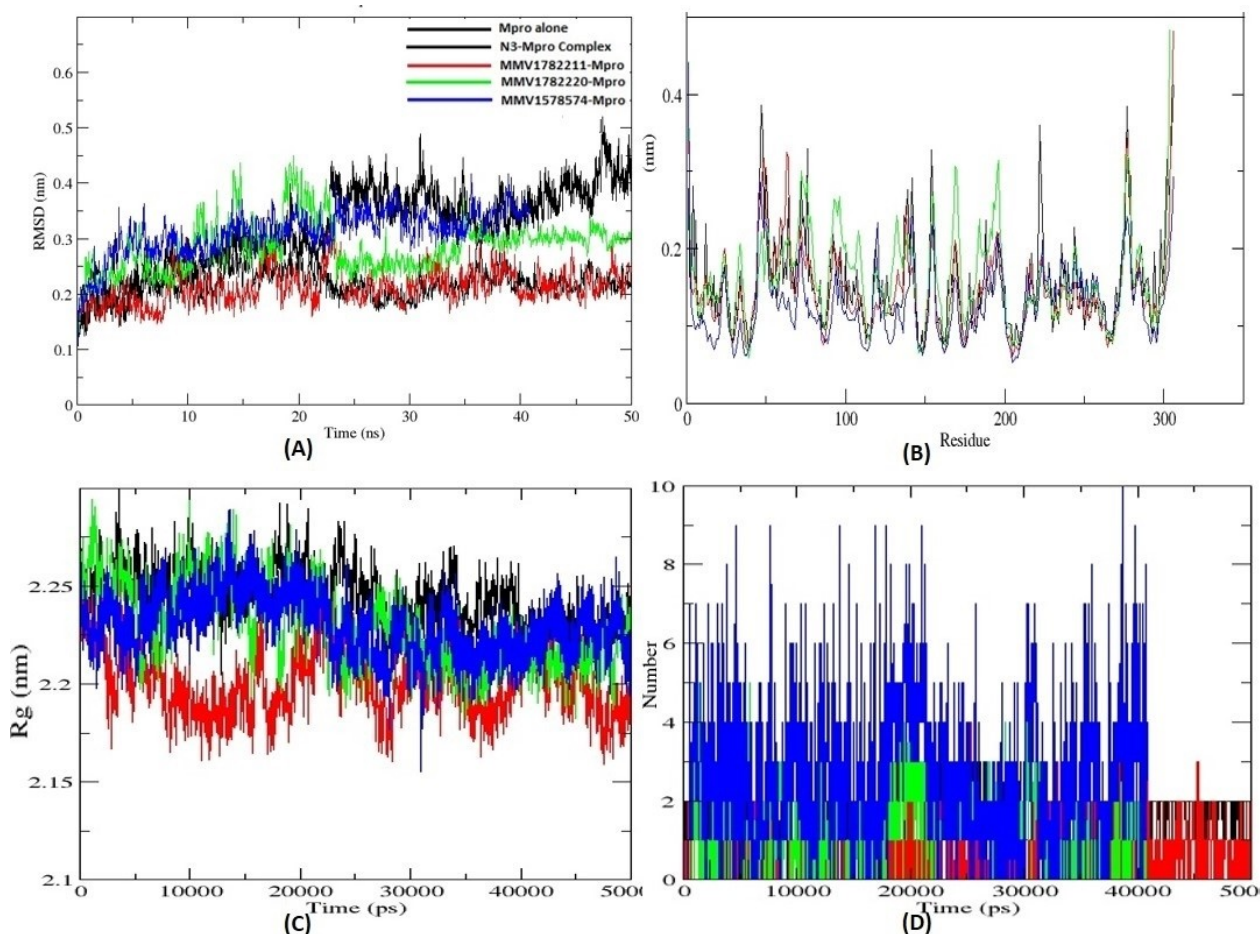
Figure 5. Comparison of molecular dynamics simulation trajectories (A) Root mean square deviation, (B) Root mean square fluctuations, (C) Radius of gyration, and (D) Number of hydrogen bond formation, for M^{pro} protein docked with the reference ligand N3 (black), MMV1782211 (red), MMV1782220 (green), and MMV1578574 (blue) over the 50 ns simulations. The trajectory graphs are developed using XMGRACE tool.

ARG40, HIS41, THR45, GLY143, CYS145, VAL 148, MET162, PRO168, ALA206 and LEU286, present in the core region have less fluctuations about the average position (0.17 nm) compared to the residues (GLU47, ASP48 MET49, TYR154, ARG222, and ASN277) present in the surface or loop regions. These results have a good coherence with crystallographic data of the protein.

Furthermore, the radius of gyration (R_g) is used to study a protein's overall conformational shape and compactness. The radius of gyration showed no abnormal behavior throughout the simulation (*Figure 5(C)*). The M^{pro}-MMV1782211 complex showed more compactness in terms of the distribution of mass around the central axis as compared with the reference and other ligands.

Hydrogen bonding is a good measure of the stability of a protein-ligand complex. Intramolecular and intermolecular hydrogen bonds play a vital role in the molecular recognition, stability, and overall conformation. The number of hydrogen bonds varies from 1–10, with an average of 2.5 during the entire simulations (*Figure 5(D)*). Solvent accessible surface area also varies for different ligands and varies 2–10 nm^2 with an average of 0.6 nm^2 per residue. It is also noted that residues in the active site region of the protein-ligand complex have a low solvent-accessible surface compared to others.

3.8. MM-PBSA Free Energy Decomposition

The MM-PBSA is a popular method for predicting the free energy of binding due to its good accuracy compared to most other scoring functions of molecular docking methods.[36] MM-PBSA based binding free energy of all protein-ligands complexes was calculated for the last 50 ns trajectories. The binding free energy was calculated using polar and apolar solvation energy. The free binding energy was investigated as electrostatic energy, polar solvation energy, van der Waals energy, SASA energy, and average binding energy (*Table 3*). The reference compound N3 showed free binding energy of −115.8 kJ/mol, whereas MMV1782211, MMV1782220, and MMV1578574

showed binding energy of −171, −143, and −118 kJ/mol suggesting MMV1782211 have the highest binding affinity for SARS-CoV-2 M^{pro} protein. Binding Energy of all ligands with protein during MD simulation showed that the binding energy of MMV1782211 is lowest altogether during the entire simulation run, which is visible in red color in *Figure 6(B)*.

The energy contribution of individual amino acid residues was also calculated using the MM-PBSA method (*Figure 6(C)*). The residue peaks in the negative Y-axis are responsible for the interaction and stability of ligands. The interacting amino acid residues such as THR24-26, HIS41, MET49, PHE140, LEU141, GLY143, SER144, CYS145, HIS163-164, MET165, GLU166, PRO168, HIS172, ASP187, ARG188, GLN189, THR190, ALA191, and GLN192 were found to surround the ligands within a distance of 4 Å.

The main protease of the SARS-CoV-2 plays a crucial role in the virus infections cycle due to its contribution in establishing a replication-transcription complex. Disrupting the normal activity of M^{pro} protein will able to halt the progression of the virus. Based on these observations, various studies have focused M^{pro} as an essential target for exploring possible interventions against SARS-CoV-2. Different investigations explored a wide range of molecules such as alkaloids,[37] plant-derived antiviral compounds,[38] plant-derived natural compounds,[39] FDA-approved antiviral drugs,[40] synthetic ligands derived from coumarins and quinolines,[41] and tested their binding efficiency against the main protease of SARS-CoV-2. Although some of the results were promising, most were yet to be tested *in vitro* or *in vivo* for efficacy. Recently, another independent in-silico study screened malaria box compounds and proposed MB 241, MB 250, and MB 266 best molecules against M^{pro} activity.[42] The present investigation exploring the antiviral and antibacterial compounds from the pathogen box of Medicines for Malaria Venture revealed significant binding efficiency of MMV178221, MMV1782220, and MMV1578574. The detailed information about identified three potent compounds is provided in *Table 4*. MMV1782211 aka TTP-8307 is previously reported as

Table 3. Van der Waals, electrostatic, polar solvation, SASA, and binding energy in kJ/mol for each M^{pro} - drug complex.

Compound ID	Van der Waals energy	Electrostatic energy	Polar solvation energy	SASA energy	Binding energy
N3	−181±26.0	−34.4±13.5	118±31.9	−18.4±2.9	−115.8±3.5
MMV1782211	−219±0.88	−22.2±0.4	89.6±.74	−19.7±.07	−171±0.9
MMV1782220	−195±16.4	−17±8.4	87.9±16.1	−18.5±1.4	−143±19.2
MMV1578574	−158±0.4	−18.8±9.0	72.6±19.0	−14.2±2.0	−118±17.3
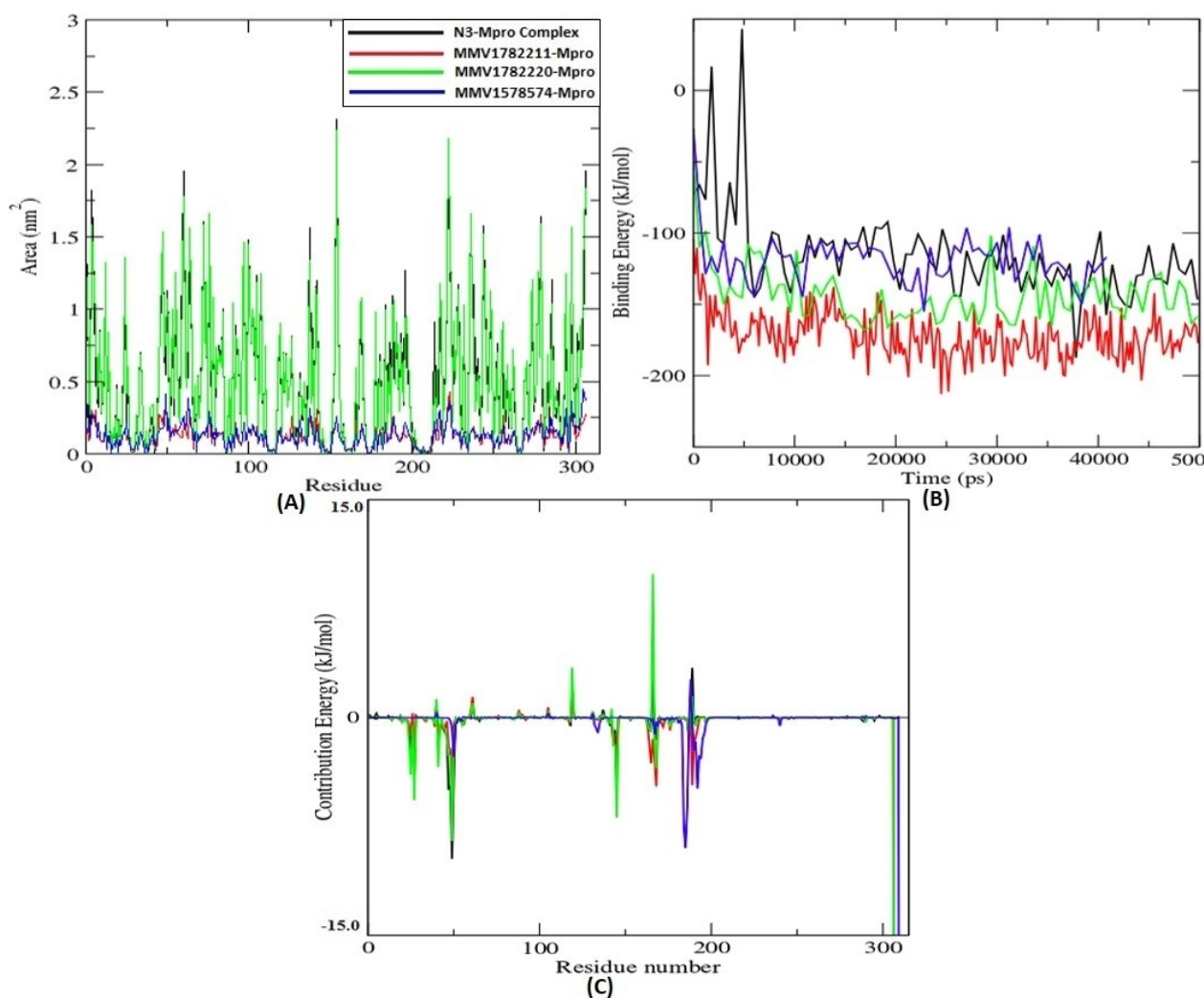
Figure 6. (A) Area per residue over the trajectory (B) Binding free energy components (C) Contribution of residues to the binding energy of M^pro protein docked with the reference ligand N3, MMV178221, MMV1782220, and MMV1578574. XMGRACE tool is used to prepare the graphs.

Table 4. Information regarding the identified compounds against M^pro drug target of SARS-CoV-2.

Compound ID	ChEMBL ID	Trivial Names	Activity
MMV1782211	CHEMBL1163676	TTP 8307	Antiviral (Rhino- and enteroviruses)
MMV1782220	CHEMBL265948	Cyclopropavir, Filociclovir, MBX-400	Antiviral (Cytomegalovirus Infection)
MMV1578574	CHEMBL1951095	Eravacycline	Antibacterial (Human intra-abdominal infections)

an antiviral compound which disrupts the replication of several rhino- and enteroviruses. The compound binds to the oxysterol-binding protein (OSBP) and disrupts its lipid shuttling function.[43,44] MMV1782220 aka MBX-400 is also an antiviral agent which is under investigation in clinical trials. The safety and pharma-

cokinetics of single oral doses of MBX-400 in healthy volunteers is completed in cytomegalovirus infection. This is a nucleoside analog that disrupts the UL97 kinase activity in cytomegalovirus.[45,46] In contrast to other two compounds, MMV1578574 aka Eravacycline is a FDA approved drug of the tetracycline antibiotic

class with a broad spectrum of activity that has demonstrated efficacy in the treatment of complicated intra-abdominal infections.[47] However, laboratory and animal studies are required to validate inhibitory role of our findings.

4. Conclusion

COVID-19 has emerged as a pandemic and is responsible for enormous mortality and morbidity in the human population worldwide. However, no approved therapeutic drugs currently exist to treat the disease, the prophylactic vaccines are the only available options, but their efficacy and safety are still concerns. We aim to combat the COVID-19 crisis by utilizing the potential of SARS-CoV-2 main protease (M^{pro}) as a drug target. The superimposition of 3D structures of M^{pro} provides information on key amino acids involved in the interaction at the main binding pocket. We have screened 10 out of 400 diverse, drug-like molecules of Pathogen box based on binding affinity compared to N3, which is used as a control to cross validates screening protocol. The physicochemical properties of these compounds lie in the permissible range. Later on, these compounds are subject to docking experiments using stringent parameters where their binding affinity lies in the range of -7.9 to -8.9 kcal/mol. The structural and superimposition analysis of selected complexes reveal that a total of only 3 compounds, namely, MMV1782211, MMV1782220, and MMV1578574, were found to interact at the main active site pocket of M^{pro}. Later on, the selected complexes were subjected to molecular dynamics simulation and MM/PBSA study to investigate their intermolecular interactions, complex stability, and binding affinity by considering N3 inhibitor as a reference point. The molecular docking, simulation, and MM/PBSA results show that MMV1782211-M^{pro} complex is the most stable configuration with high free binding energy compared to N3. This compound may have the ability to block the expression of the main protease enzyme, resulting in the disruption of their replication mechanism. Hence, this compound can be further evaluated as a SARS-CoV-2 M^{pro} inhibitor using *in vitro* and *in vivo* model studies.

Acknowledgements

Conflict of Interest

The authors declare no conflict of interest.

Data Availability Statement

Research data are not shared.

Author Contribution Statement

R.T., A.P., K.K.O. and M.K.Y. performed the experiments, analyzed the data and wrote the article. M.K.Y., S.K., A.K.P. and A.C. contributed in the methodology part and analyzed the data. R.T., V.S.R., M.K.Y. and S.K. conceived and designed the experiments. V.S.R., S.K. and M.K.Y. prepared the original draft.

References

[1] J. F. Chan, K. H. Kok, Z. Zhu, H. Chu, K. K. To, S. Yuan, K. Y. Yuen, 'Genomic characterization of the 2019 novel human-pathogenic coronavirus isolated from a patient with atypical pneumonia after visiting Wuhan', *Emerg. Microbes Infect.* **2020**, *9*, 221–236.

[2] J. F.-W. Chan, S. Yuan, K.-H. Kok, K. K.-W. To, H. Chu, J. Yang, F. Xing, J. Liu, C. C.-Y. Yip, R. W.-S. Poon, H.-W. Tsoi, S. K.-F. Lo, K.-H. Chan, V. K.-M. Poon, W.-M. Chan, J. D. Ip, J.-P. Cai, V. C.-C. Cheng, H. Chen, C. K.-M. Hui, K.-Y. Yuen, 'A familial cluster of pneumonia associated with the 2019 novel coronavirus indicating person-to-person transmission: a study of a family cluster', *The Lancet* **2020**, *395*, 514–523.

[3] N. Chen, M. Zhou, X. Dong, J. Qu, F. Gong, Y. Han, Y. Qiu, J. Wang, Y. Liu, Y. Wei, J. A. Xia, T. Yu, X. Zhang, L. Zhang, 'Epidemiological and clinical characteristics of 99 cases of 2019 novel coronavirus pneumonia in Wuhan, China: a descriptive study', *The Lancet* **2020**, *395*, 507–513.

[4] D. Cucinotta, M. Vanelli, 'WHO Declares COVID-19 a Pandemic', *Acta. Biomed.* **2020**, *91*, 157–160.

[5] B. A. C. Rattis, S. G. Ramos, M. R. N. Celes, 'Curcumin as a Potential Treatment for COVID-19', *Front. Pharmacol.* **2021**, *12*, 1–14.

[6] A. Vahedian-Azimi, M. Abbasifard, F. Rahimi-Bashar, P. C. Guest, M. Majeed, A. Mohammadi, M. Banach, T. Jamialahmadi, A. Sahebkar, 'Effectiveness of Curcumin on Outcomes of Hospitalized COVID-19 Patients: A Systematic Review of Clinical Trials', *Nutrients* **2022**, *14*, 256.

[7] A. B. Jena, N. Kanungo, V. Nayak, G. B. N. Chainy, J. Dandapat, 'Catechin and curcumin interact with S protein of SARS-CoV2 and ACE2 of human cell membrane: insights from computational studies', *Sci. Rep.* **2021**, *11*, 1–14.

[8] A. B. Jena, N. Kanungo, G. B. N. Chainy, V. Devaraji, S. K. Das, J. Dandapat, 'A Computational Insight on the Inhibitory Potential of 8-Hydroxydihydrosanguinarine (8-HDS), a Pyridone Containing Analog of Sanguinarine, against SARS CoV2', *Chem. Biodiversity* **2022**, *19*, 1–14.

[9] Z. Ren, L. Yan, N. Zhang, Y. Guo, C. Yang, Z. Lou, Z. Rao, 'The newly emerged SARS-like coronavirus HCoV-EMC also has an" Achilles' heel": current effective inhibitor targeting a 3 C-like protease', *Protein Cell* **2013**, *4*, 248–250.

[10] Z. Jin, X. Du, Y. Xu, Y. Deng, M. Liu, Y. Zhao, B. Zhang, X. Li, L. Zhang, C. Peng, 'Structure of Mpro from SARS-CoV-2 and discovery of its inhibitors', *Nature* **2020**, *582*, 289–293.

[11] T. Klemm, G. Ebert, D. J. Calleja, C. C. Allison, L. W. Richardson, J. P. Bernardini, B. G. Lu, N. W. Kuchel, C. Grohmann, Y. Shibata, Z. Y. Gan, J. P. Cooney, M. Doerflinger, A. E. Au, T. R. Blackmore, G. J. van der Heden van Noort, P. P. Geurink, H. Ovaa, J. Newman, A. Riboldi-Tunnicliffe, P. E. Czabotar, J. P. Mitchell, R. Feltham, B. C. Lechtenberg, K. N. Lowes, G. Dewson, M. Pellegrini, G. Lessene, D. Komander, 'Mechanism and inhibition of the papain-like protease, PLpro, of SARS-CoV-2', *EMBO J.* **2020**, *39*, e106275.

[12] A. Hegyi, J. Ziebuhr, 'Conservation of substrate specificities among coronavirus main proteases', *J. Gen. Virol.* **2002**, *83*, 595–599.

[13] Umesh, D. Kundu, C. Selvaraj, S. K. Singh, V. K. Dubey, 'Identification of new anti-nCoV drug chemical compounds from Indian spices exploiting SARS-CoV-2 main protease as target', *J. Biomol. Struct. Dyn.* **2021**, *39*, 3428–3434.

[14] M. Hoffmann, K. Mösbauer, H. Hofmann-Winkler, A. Kaul, H. Kleine-Weber, N. Krüger, N. C. Gassen, M. A. Müller, C. Drosten, S. Pöhlmann, 'Chloroquine does not inhibit infection of human lung cells with SARS-CoV-2', *Nature* **2020**, *585*, 588–590.

[15] S. K. Burley, C. Bhikadiya, C. Bi, S. Bittrich, L. Chen, G. V. Crichlow, C. H. Christie, K. Dalenberg, L. Di Costanzo, J. M. Duarte, S. Dutta, Z. Feng, S. Ganesan, D. S. Goodsell, S. Ghosh, R. K. Green, V. Guranović, D. Guzenko, B. P. Hudson, C. L. Lawson, Y. Liang, R. Lowe, H. Namkoong, E. Peisach, I. Persikova, C. Randle, A. Rose, Y. Rose, A. Sali, J. Segura, M. Sekharan, C. Shao, Y.-P. Tao, M. Voigt, J. D. Westbrook, J. Y. Young, C. Zardecki, M. Zhuravleva, 'RCSB Protein Data Bank: powerful new tools for exploring 3D structures of biological macromolecules for basic and applied research and education in fundamental biology, biomedicine, biotechnology, bioengineering and energy sciences', *Nucleic Acids Res.* **2020**, *49*, D437-D451.

[16] S. Günther, P. Y. A. Reinke, Y. Fernández-García, J. Lieske, T. J. Lane, H. M. Ginn, F. H. M. Koua, C. Ehrt, W. Ewert, D. Oberthuer, O. Yefanov, S. Meier, K. Lorenzen, B. Krichel, J. D. Kopicki, L. Gelisio, W. Brehm, I. Dunkel, B. Seychell, H. Gieseler, B. Norton-Baker, B. Escudero-Pérez, M. Domaracky, S. Saouane, A. Tolstikova, T. A. White, A. Hänle, M. Groessler, H. Fleckenstein, F. Trost, M. Galchenkova, Y. Gevorkov, C. Li, S. Awel, A. Peck, M. Barthelmess, F. Schlünzen, P. Lourdu Xavier, N. Werner, H. Andaleeb, N. Ullah, S. Falke, V. Srinivasan, B. A. França, M. Schwinzer, H. Brognaro, C. Rogers, D. Melo, J. J. Zaitseva-Doyle, J. Knoska, G. E. Peña-Murillo, A. R. Mashhour, V. Hennicke, P. Fischer, J. Hakanpää, J. Meyer, P. Gribbon, B. Ellinger, M. Kuzikov, M. Wolf, A. R. Beccari, G. Bourenkov, D. von Stetten, G. Pompidor, I. Bento, S. Panneerselvam, I. Karpics, T. R. Schneider, M. M. Garcia-Alai, S. Niebling, C. Günther, C. Schmidt, R. Schubert, H. Han, J. Boger, D. C. F. Monteiro, L. Zhang, X. Sun, J. Pletzer-Zelgert, J. Wollenhaupt, C. G. Feiler, M. S. Weiss, E. C. Schulz, P. Mehrabi, K. Karničar, A. Usenik, J. Loboda, H. Tidow, A. Chari, R. Hilgenfeld, C. Uetrecht, R. Cox, A. Zaliani, T. Beck, M. Rarey, S. Günther, D. Turk, W. Hinrichs, H. N. Chapman, A. R. Pearson, et al., 'X-ray screening identifies active site and allosteric inhibitors of SARS-CoV-2 main protease', *Science* **2021**, *372*, 642–646.

[17] H. Yang, W. Xie, X. Xue, K. Yang, J. Ma, W. Liang, Q. Zhao, Z. Zhou, D. Pei, J. Ziebuhr, R. Hilgenfeld, K. Y. Yuen, L. Wong, G. Gao, S. Chen, Z. Chen, D. Ma, M. Bartlam, Z. Rao, 'Design of wide-spectrum inhibitors targeting coronavirus main proteases', *PLoS Biol.* **2005**, *3*, e324.

[18] E. F. Pettersen, T. D. Goddard, C. C. Huang, G. S. Couch, D. M. Greenblatt, E. C. Meng, T. E. Ferrin, 'UCSF Chimera–a visualization system for exploratory research and analysis', *J. Comput. Chem.* **2004**, *25*, 1605–1612.

[19] T. A. Binkowski, S. Naghibzadeh, J. Liang, 'CASTp: Computed Atlas of Surface Topography of proteins', *Nucleic Acids Res.* **2003**, *31*, 3352–3355.

[20] W. Tian, C. Chen, X. Lei, J. Zhao, J. Liang, 'CASTp 3.0: computed atlas of surface topography of proteins', *Nucleic Acids Res.* **2018**, *46*, 363–367.

[21] R. Rufener, L. Dick, L. D'Ascoli, D. Ritler, A. Hizem, T. N. C. Wells, A. Hemphill, B. Lundström-Stadelmann, 'Repurposing of an old drug: In vitro and in vivo efficacies of buparvaquone against Echinococcus multilocularis', *Int. J. Parasitol.: Drugs Drug Resist.* **2018**, *8*, 440–450.

[22] M. D. Hanwell, D. E. Curtis, D. C. Lonie, T. Vandermeersch, E. Zurek, G. R. Hutchison, 'Avogadro: an advanced semantic chemical editor, visualization, and analysis platform', *J. Cheminformatics* **2012**, *4*, 1–17.

[23] N. M. O'Boyle, M. Banck, C. A. James, C. Morley, T. Vandermeersch, G. R. Hutchison, 'Open Babel: An open chemical toolbox', *J. Cheminformatics* **2011**, *3*, 1–14.

[24] M. Chappell, S. Payne, in *Physiology for Engineers: Applying Engineering Methods to Physiological Systems*, Springer International Publishing, Cham, 2020, pp. 61–72.

[25] O. Trott, A. J. Olson, 'AutoDock Vina: improving the speed and accuracy of docking with a new scoring function, efficient optimization, and multithreading', *J. Comput. Chem.* **2010**, *31*, 455–461.

[26] H. M. Berman, J. Westbrook, Z. Feng, G. Gilliland, T. N. Bhat, H. Weissig, I. N. Shindyalov, P. E. Bourne, 'The Protein Data Bank', *Nucleic Acids Res.* **2000**, *28*, 235–242.

[27] G. M. Morris, R. Huey, W. Lindstrom, M. F. Sanner, R. K. Belew, D. S. Goodsell, A. J. Olson, 'AutoDock4 and AutoDockTools4: Automated docking with selective receptor flexibility', *J. Comput. Chem.* **2009**, *30*, 2785–2791.

[28] C. Oostenbrink, A. Villa, A. E. Mark, W. F. van Gunsteren, 'A biomolecular force field based on the free enthalpy of hydration and solvation: the GROMOS force-field parameter sets 53 A5 and 53 A6', *J. Comput. Chem.* **2004**, *25*, 1656–1676.

[29] S. Pronk, S. Páll, R. Schulz, P. Larsson, P. Bjelkmar, R. Apostolov, M. R. Shirts, J. C. Smith, P. M. Kasson, D. van der Spoel, B. Hess, E. Lindahl, 'GROMACS 4.5: a high-throughput and highly parallel open source molecular simulation toolkit', *Bioinformatics* **2013**, *29*, 845–854.

[30] J. A. Lemkul, W. J. Allen, D. R. Bevan, 'Practical considerations for building GROMOS-compatible small-molecule topologies', *J. Chem. Inf. Model.* **2010**, *50*, 2221–2235.

[31] K. Vollmayr-Lee, 'Introduction to molecular dynamics simulations', *Am. J. Phys.* **2020**, *88*, 401–422.

[32] B. Hess, H. Bekker, H. J. C. Berendsen, J. G. E. M. Fraaije, 'LINCS: A linear constraint solver for molecular simulations', *J. Comput. Chem.* **1997**, *18*, 1463–1472.

[33] A. Toukmaji, C. Sagui, J. Board, T. Darden, 'Efficient particle-mesh Ewald based approach to fixed and induced dipolar interactions', *J. Chem. Phys.* **2000**, *113*, 10913–10927.

[34] P. Turner, 'XMGRACE, Version 5.1.19', *Beaverton, OR: Center for Coastal and Land-Margin Research, Oregon Graduate Institute of Science and Technology* **2005**.

[35] E. R. Lusczek, N. E. Ingraham, B. S. Karam, J. Proper, L. Siegel, E. S. Helgeson, S. Lotfi-Emran, E. J. Zolfaghari, E. Jones, M. G. Usher, 'Characterizing COVID-19 clinical phenotypes and associated comorbidities and complication profiles', *PloS one* **2021**, *16*, e0248956.

[36] E. Wang, H. Sun, J. Wang, Z. Wang, H. Liu, J. Z. H. Zhang, T. Hou, 'End-Point Binding Free Energy Calculation with MM/PBSA and MM/GBSA: Strategies and Applications in Drug Design', *Chem. Rev.* **2019**, *119*, 9478–9508.

[37] S. Garg, A. Roy, 'In silico analysis of selected alkaloids against main protease (Mpro) of SARS-CoV-2', *Chem. Biol. Interact.* **2020**, *332*, 1–12.

[38] A. Sharma, S. Goyal, A. K. Yadav, P. Kumar, L. Gupta, 'In-silico screening of plant-derived antivirals against main protease, 3CLpro and endoribonuclease, NSP15 proteins of SARS-CoV-2', *J. Biomol. Struct. Dyn.* **2020**, 1–15.

[39] D. M. Teli, M. B. Shah, M. T. Chhabria, 'In silico Screening of Natural Compounds as Potential Inhibitors of SARS-CoV-2 Main Protease and Spike RBD: Targets for COVID-19', *Front. Mol. Biosci.* **2021**, *7*, 1–25.

[40] Y. Kumar, H. Singh, C. N. Patel, 'In silico prediction of potential inhibitors for the main protease of SARS-CoV-2 using molecular docking and dynamics simulation based drug-repurposing', *J. Infect. Public Health* **2020**, *13*, 1210–1223.

[41] O. Yañez, M. I. Osorio, E. Uriarte, C. Areche, W. Tiznado, J. M. Pérez-Donoso, O. García-Beltrán, F. González-Nilo, '*In Silico* Study of Coumarins and Quinolines Derivatives as Potent Inhibitors of SARS-CoV-2 Main Protease', *Front. Chem.* **2021**, *8*, 1–15.

[42] S. Ahamad, H. Kanipakam, S. Birla, M. S. Ali, D. Gupta, 'Screening Malaria-box compounds to identify potential inhibitors against SARS-CoV-2 Mpro, using molecular docking and dynamics simulation studies', *Eur. J. Pharmacol.* **2021**, *890*, 1–12.

[43] L. Albulescu, J. Bigay, B. Biswas, M. Weber-Boyvat, C. M. Dorobantu, L. Delang, H. M. van der Schaar, Y. S. Jung, J. Neyts, V. M. Olkkonen, F. J. M. van Kuppeveld, J. Strating, 'Uncovering oxysterol-binding protein (OSBP) as a target of the anti-enteroviral compound TTP-8307', *Antivir. Res.* **2017**, *140*, 37–44.

[44] A. M. D. Palma, H. J. Thibaut, L. v. d. Linden, K. Lanke, W. Heggermont, S. Ireland, R. Andrews, M. Arimilli, T. H. Al-Tel, E. D. Clercq, F. v. Kuppeveld, J. Neyts, 'Mutations in the Nonstructural Protein 3 A Confer Resistance to the Novel Enterovirus Replication Inhibitor TTP-8307', *Antimicrob. Agents Chemother.* **2009**, *53*, 1850–1857.

[45] S. H. James, C. B. Hartline, E. A. Harden, E. M. Driebe, J. M. Schupp, D. M. Engelthaler, P. S. Keim, T. L. Bowlin, E. R. Kern, M. N. Prichard, 'Cyclopropavir inhibits the normal function of the human cytomegalovirus UL97 kinase', *Antimicrob. Agents Chemother.* **2011**, *55*, 4682–4691.

[46] N. G. Rouphael, S. J. Hurwitz, M. Hart, A. Beck, E. J. Anderson, G. Deye, B. Osborn, S. Y. Cai, C. Focht, C. Amegashie, T. L. Bowlin, J. Brooks, M. J. Mulligan, 'Phase Ib Trial To Evaluate the Safety and Pharmacokinetics of Multiple Ascending Doses of Filociclovir (MBX-400, Cyclopropavir) in Healthy Volunteers', *Antimicrob. Agents Chemother.* **2019**, *63*, e00717–00719.

[47] M. Heaney, M. V. Mahoney, J. C. Gallagher, 'Eravacycline: The Tetracyclines Strike Back', *Ann. Pharmacother.* **2019**, *53*, 1124–1135.